PTEP

Prog. Theor. Exp. Phys. **2017**, 12A105 (20 pages)
DOI: 10.1093/ptep/ptx021

Origin of Ultra High Energy Cosmic Rays

IceCube: Neutrinos and multimessenger astronomy

Markus Ahlers and Francis Halzen*

Wisconsin IceCube Particle Astrophysics Center (WIPAC) and Department of Physics, University of Wisconsin-Madison, Madison, WI 53706, USA
*E-mail: halzen@icecube.wisc.edu

Received January 19, 2017; Revised February 2, 2017; Accepted February 6, 2017; Published November 29, 2017

We review the status of the IceCube observations of cosmic neutrinos. We investigate model-independent constraints on the properties of the sources where they originate. Specifically, we evaluate the multimessenger relations connecting neutrino, gamma ray, and cosmic ray observations and conclude that neutrinos are ubiquitous in the nonthermal universe, suggesting a more significant role than previously anticipated. Subsequently, we study the implications of IceCube's upper limits on the flux from individual point sources, as well as on the "guaranteed" flux of cosmogenic neutrinos.

Subject Index B74, E41, E44, E45

1. Introduction: Multimessenger astronomy

With the commissioning of the IceCube [1,2] and Advanced LIGO [3] facilities, we are able to observe the universe for the first time using three distinct astronomical messengers. In addition to photons, from radio waves to gamma rays, we can now simultaneously observe the sky with gravitational waves and high-energy neutrinos. This new era of multimessenger astrophysics will offer a unique view of our universe and provide powerful insights into the workings of some of the most energetic and enigmatic objects in the cosmos. In fact, initial findings have been astonishing. The first direct observation of a gravitational wave may become a footnote in history to the fact that thirty-solar-mass black holes exist to generate its energy. The mere existence of black holes with such a mass challenges our understanding of the universe.

Powered by gravity, shocks in the relativistic particle flows in the vicinity of neutron stars and black holes may transform a fraction of the gravitational energy into the acceleration of particles, mostly protons that are observed as cosmic rays. We do not know how, or even where, this happens, but we have detected cosmic rays with Joule kinetic energy that bear witness to the enigmatic processes that pack a macroscopic energy into a single elementary particle.

With IceCube's discovery that neutrinos from the cosmos can be observed with a cubic kilometer detector, cosmic neutrinos may now reveal an unobstructed view of the universe at wavelengths above tens of TeV where the universe is opaque to light. With more than one thousand times the energy of the highest-energy neutrinos produced with earthbound accelerators, cosmic neutrinos also exceed by a factor of one billion the energy of the neutrinos detected from a supernova that

exploded in the Large Magellanic Cloud in February 1987, the only neutrinos that have reached us from outside the solar system prior to IceCube's breakthrough. It is therefore probably somewhat counterintuitive that the more puzzling property of the observed cosmic neutrinos is not their energy but their large intensity.

An immediate inference made about the large neutrino flux observed by IceCube, which is predominantly extragalactic in origin, is that the total energy density of neutrinos in the high-energy universe is similar to that of gamma rays. This is worthy of a closer look. Neutrinos are the decay products of pions. Protons accelerated in regions of high magnetic fields near neutron stars or black holes may interact with the radiation or dust surrounding them to produce pions and kaons that decay into neutrinos. This is the mechanism by which neutrino beams are produced at Fermilab, where the target material is arranged to be sufficiently dense so as to absorb all secondary particles created in the collisions, except for the neutrinos of course. Not so in the sky, where pions and kaons are produced in more tenuous radiation fields or in dust in the vicinity of the accelerator. In fact, the accelerator and the pion-producing target may be separated, as is the case for the abundant production of gamma rays in the Galactic plane. Elementary particle physics dictates that neutral pions, which promptly decay into two gamma rays, inevitably accompany charged pions generating neutrinos.

It seems, therefore, surprising that no gamma ray has ever been observed matching the 100 to 10,000 TeV energy range of IceCube neutrinos. However, this is just a consequence of the universe's opacity to high-energy photons. Unlike neutrinos, gamma rays interact with photons of the cosmic microwave background before reaching Earth. The resulting electromagnetic shower subdivides the initial photon energy, resulting in multiple photons in the GeV–TeV energy range by the time the shower reaches Earth. Calculating the cascaded gamma ray flux accompanying IceCube neutrinos is straightforward. It is intriguing that the the resulting flux shown in Fig. 1 matches the extragalactic high-energy gamma ray flux observed by the Fermi satellite.

The matching energy densities of the extragalactic gamma ray flux detected by Fermi and the high-energy neutrino flux measured by IceCube suggest that, rather than detecting some exotic sources, it is more likely that IceCube to a large extent observes the same universe astronomers do. The finding implies that a large fraction, possibly most, of the energy in the nonthermal universe originates in hadronic processes, indicating a larger role than previously thought. IceCube is developing methods, most promisingly real-time multiwavelength observations with astronomical telescopes, to identify the sources and build on the discovery of cosmic neutrinos to launch a new era in astronomy [7,8].

The outline of this paper is as follows. After briefly introducing IceCube in Sect. 2, we will review the status of its observations in Sect. 3. Subsequently, we will discuss the initial lessons learned for multimessenger astronomy in Sect. 4. The nonobservation of extragalactic neutrino point sources allows the placement of exclusion limits on the density of feasible point source populations, as we will discuss in Sect. 5. We then discuss the possibility that the sources of ultra-high-energy cosmic rays (UHE CRs) are related to the observed flux of cosmic neutrinos in Sect. 6. In Sect. 7, we review the predictions of cosmogenic neutrinos, which are considered a "guaranteed" contribution of the sources of UHE CRs. We finally consider the possibility of finding correlations of UHE CR events with neutrino events in Sect. 8 before we conclude in Sect. 9.

2. IceCube

The IceCube detector [1] transforms deep natural Antarctic ice 1450 m below the geographic South Pole into a Cherenkov detector. The instrument consists of 5160 digital optical modules that instrument a cubic kilometer of ice; see Fig. 2. Each digital optical module consists of a glass sphere that

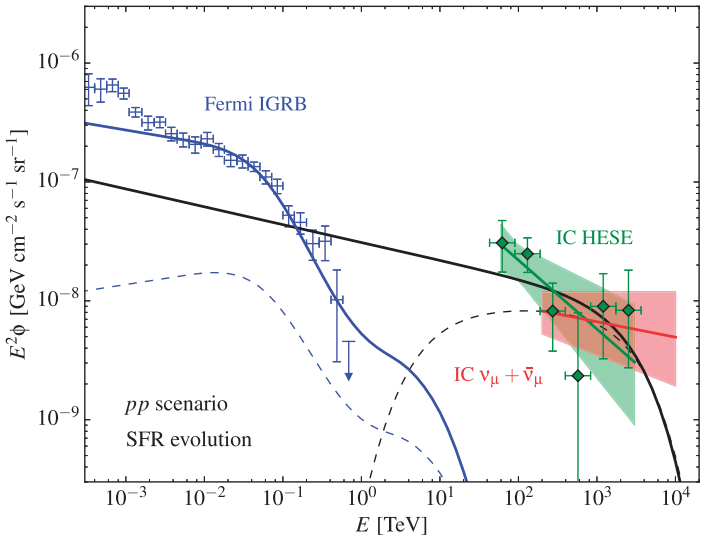

Fig. 1. Two models of the astrophysical neutrino flux (black lines) observed by IceCube and the corresponding cascaded gamma ray flux (blue lines) observed by Fermi. The models assume that the decay products of neutral and charged pions from *pp* interactions are responsible for the nonthermal emission in the universe [4]. The thin dashed lines represent an attempt to minimize the contribution of the pionic gamma ray flux to the Fermi observations. It assumes an injected flux of E^{-2} with exponential cutoff at low and high energy. The green data show the binned neutrino spectrum inferred from the four-year "high-energy starting event" (HESE) analysis [5]. The green solid line and shaded band indicate the corresponding power-law fit with uncertainty range. Also shown as a red solid line and shaded band is the best fit to the flux of high-energy muon neutrinos penetrating the Earth [6].

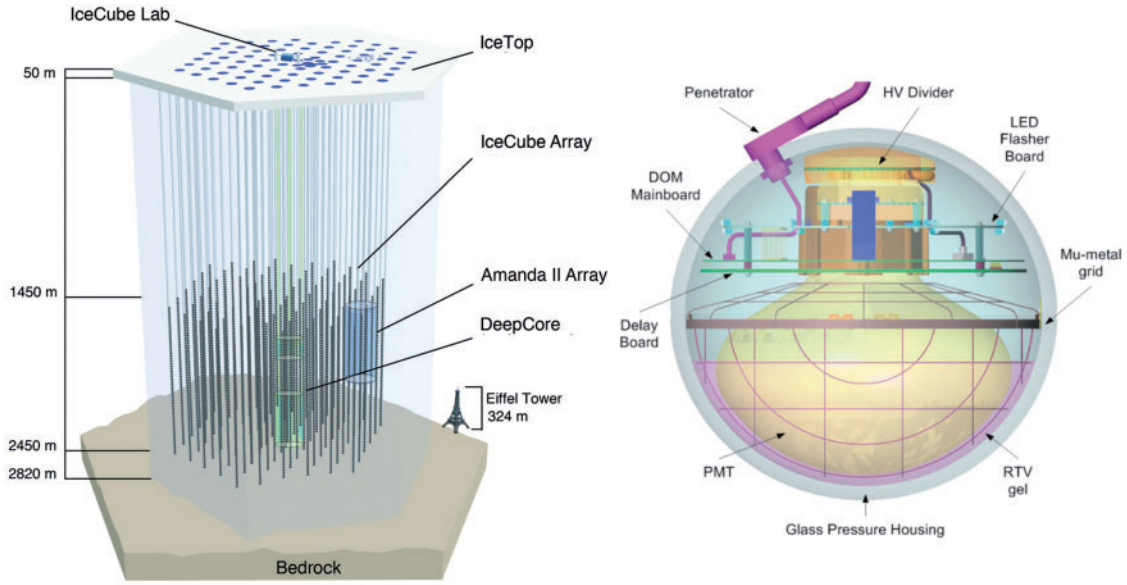

Fig. 2. Architecture of the IceCube observatory (left) and the schematics of a digital optical module (right).

contains a 10 in photomultiplier and the electronics board that digitizes the signals locally using an onboard computer. The digitized signals are given a global time stamp with residuals accurate to 2 ns and are subsequently transmitted to the surface. Processors at the surface continuously collect the time-stamped signals from the optical modules, each of which functions independently. These

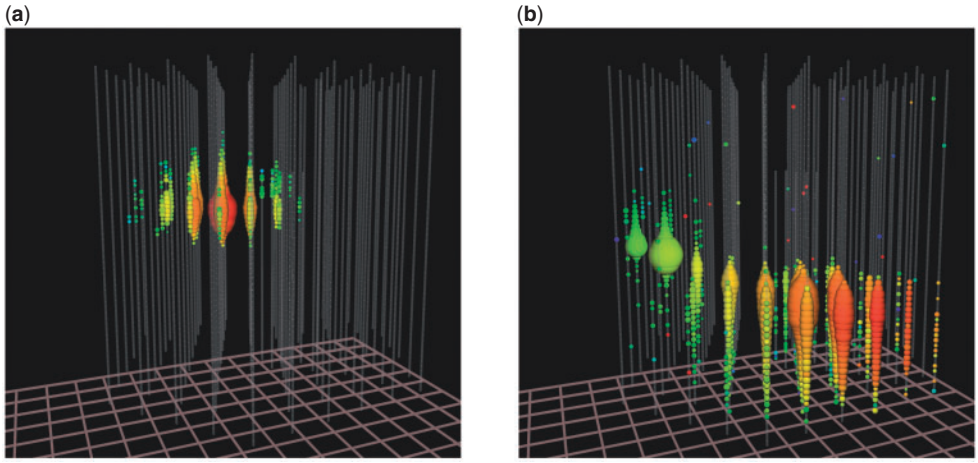

Fig. 3. (a) Light pool produced in IceCube by a shower initiated by an electron or tau neutrino. The measured energy is 1.14 PeV, which represents a lower limit on the energy of the neutrino that initiated the shower. White dots represent sensors with no signal. For the colored dots, the color indicates arrival time, from red (early) to purple (late) following the rainbow, and size reflects the number of photons detected. (b) An upgoing muon track traverses the detector at an angle of 11° below the horizon. The deposited energy inside the detector is 2.6 PeV.

signals are sorted into telltale patterns of light that reveal the direction, energy, and flavor of the incident neutrino.

Even at a depth of 1450 m, IceCube detects a background of atmospheric cosmic ray muons originating in the Southern Hemisphere at a rate of 3000 per second. Two methods are used to identify neutrinos. Traditionally, neutrino searches have focused on the observation of muon neutrinos that interact primarily outside the detector to produce kilometer-long muon tracks passing through the instrumented volume. Although this allows the identification of neutrinos that interact outside the detector, it is necessary to use the Earth as a filter in order to remove the huge background of cosmic ray muons. This limits the neutrino view to a single flavor and half the sky. An alternative method exclusively identifies neutrinos interacting inside the detector [9]. It divides the instrumented volume of ice into an outer veto shield and a 500-megaton inner fiducial volume. The advantage of focusing on neutrinos interacting inside the instrumented volume of ice is that the detector functions as a total absorption calorimeter, measuring the neutrino energy with a 10%–15% resolution. Furthermore, with this method, neutrinos from all directions in the sky can be identified, including both muon tracks as well as secondary showers, produced by charged-current interactions of electron and tau neutrinos, and neutral current interactions of neutrinos of all flavors. The Cherenkov patterns initiated by an electron (or tau) neutrino of 1 PeV energy and a muon neutrino depositing 2.6 PeV energy while traversing the detector are contrasted in Fig. 3.

In general, the arrival times of photons at the optical sensors determine the particle's trajectory [10], while the number of photons is a proxy for the deposited energy. The two methods for separating neutrinos from the cosmic ray muon background have complementary advantages. The long tracks produced by muon neutrinos can be pointed back to their sources with a $\leq 0.4°$ angular resolution. In contrast, the reconstruction of the direction of secondary showers, in principle possible to a few degrees, is still in the development stage in IceCube [11]. They can be pointed to within $\sim$10°–15° of the direction of the incident neutrino. Determining the deposited energy from the observed light pool is, however, relatively straightforward, and a resolution of better than 15% is possible; the same value holds for the reconstruction of the energy deposited by a muon track inside the detector.

3. Cosmic neutrinos

For neutrino astronomy, the first challenge is to select a pure sample of neutrinos, roughly 100,000 per year above a threshold of 0.1 TeV for IceCube, in a background of ten billion cosmic ray muons, while the second is to identify the small fraction of these neutrinos that is astrophysical in origin, observed at the level of tens of events per year. Atmospheric neutrinos are an overwhelming background for cosmic neutrinos, at least at energies below ∼100 TeV. Above this energy, however, the atmospheric neutrino flux is too low to produce events, even in a kilometer-scale detector, and events in that energy range are cosmic in origin.

Using the Earth as a filter, a flux of neutrinos has been identified that is predominantly of atmospheric origin. IceCube has measured this flux over three orders of magnitude in energy with a result that is consistent with theoretical calculations [12,13]. However, in seven years of data, an excess of events is observed at energies beyond 100 TeV [6,14], which cannot be accommodated by the atmospheric flux; see Fig. 4. Allowing for large uncertainties on the extrapolation of the atmospheric component, the statistical significance of the excess astrophysical flux is $6\,\sigma$. While IceCube measures only the energy deposited by the secondary muon inside the detector, from Standard Model physics we can infer the energy spectrum of the parent neutrinos represented in the figure. For the highest-energy event, already shown in Fig. 3, the most likely energy of the parent neutrino approaches 10 PeV. Independent of any calculation, the energy lost by the muon inside the instrumented detector volume is 2.6 ± 0.3 PeV. The cosmic neutrino flux is well described by a power law with a spectral index $\gamma = 2.13 \pm 0.13$ and a normalization at 100 TeV neutrino energy of $(0.90^{+0.30}_{-0.27}) \times 10^{-18}\,\mathrm{GeV}^{-1}\,\mathrm{cm}^{-2}\,\mathrm{s}^{-1}\mathrm{sr}^{-1}$ [6]. The error range is estimated from a profile likelihood using Wilks' theorem and includes both statistical and systematic uncertainties. The neutrino energy contributing to this flux covers the range 200 TeV to 9 PeV.

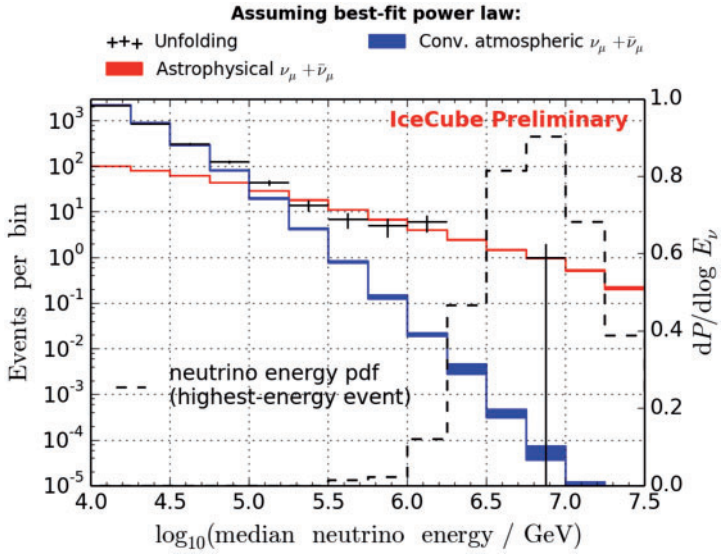

Fig. 4. Spectrum of secondary muons initiated by muon neutrinos that have traversed the Earth, i.e., with zenith angle less than 5° above the horizon, as a function of the energy they deposit inside the detector. For each reconstructed muon energy, the median neutrino energy is calculated assuming the best-fit spectrum. The colored bands (blue/red) show the expectation for the conventional and astrophysical contributions. The black crosses show the measured data. Additionally, the neutrino energy probability density function for the highest-energy event assuming the best-fit spectrum is shown (dashed line).

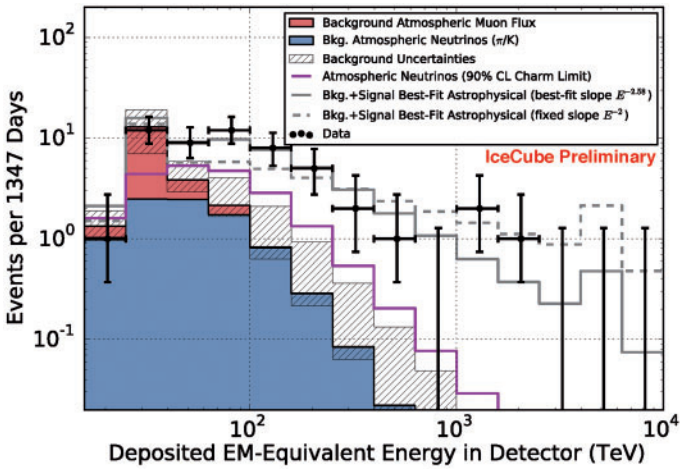

Fig. 5. Deposited energies of muons observed in four years of data [5]. The hashed region shows uncertainties on the sum of all backgrounds. The atmospheric muon flux (red) and its uncertainty is computed from simulation to overcome statistical limitations in our background measurement and scaled to match the total measured background rate. The atmospheric neutrino flux is derived from previous measurements of both the π, K, and charm components of the atmospheric spectrum [25]. Also shown are two illustrative power-law fits to the spectrum.

However, it was the alternative method, which selects isolated neutrinos interacting inside the detector, that revealed the first evidence for cosmic neutrinos [15,16]. Their isolation and well-measured energy allows for a clear separation between neutrinos of atmospheric origin and those of cosmic origin; a sample event with a light pool of roughly 100,000 photoelectrons extending over more than 500 m is shown in Fig. 3. The geometry of the veto and active signal regions has been optimized to reduce the background of atmospheric muons and neutrinos to a handful of events per year while keeping 98% of the cosmic signal.

With PeV energy and no trace of accompanying muons from an atmospheric shower, these events are highly unlikely to be of atmospheric origin. It is indeed important to realize that the muon produced in the same pion or kaon decay as an atmospheric neutrino will reach the detector provided that the neutrino energy is sufficiently high and the zenith angle sufficiently small [9,17]. PeV atmospheric neutrinos come with their own self-veto. This self-veto is applied to IceCube cosmic neutrino candidates that exclusively consist of isolated neutrino events.

The energy dependence of the high-energy neutrinos collected in four years of data [5] is compared to that of atmospheric backgrounds in Fig. 5. It is, above an energy of 200 TeV, consistent with the flux of muon neutrinos penetrating the Earth shown in Fig. 4. A purely atmospheric explanation of the observation is excluded at $7\,\sigma$.

In summary, IceCube has observed cosmic neutrinos using both methods for rejecting background; each analysis has reached a statistical significance of more than $6\,\sigma$. Based on different methods for reconstruction and energy measurement, their results agree, pointing at extragalactic sources whose flux has equilibrated in the three flavors after propagation over cosmic distances [18] with $\nu_e : \nu_\mu : \nu_\tau \sim 1 : 1 : 1$. Its total energy matches that of extragalactic photons, as seen in Fig. 1, and also that of UHE CRs, as we will discuss in one of the following sections.

The four-year data set contains a total of 54 neutrino events with deposited energies ranging from 30 to 2000 TeV. The data in both Figs. 4 and 5 support an astrophysical component with a spectrum close to E^{-2} above an energy of ~ 200 TeV. An extrapolation of this high-energy flux to lower

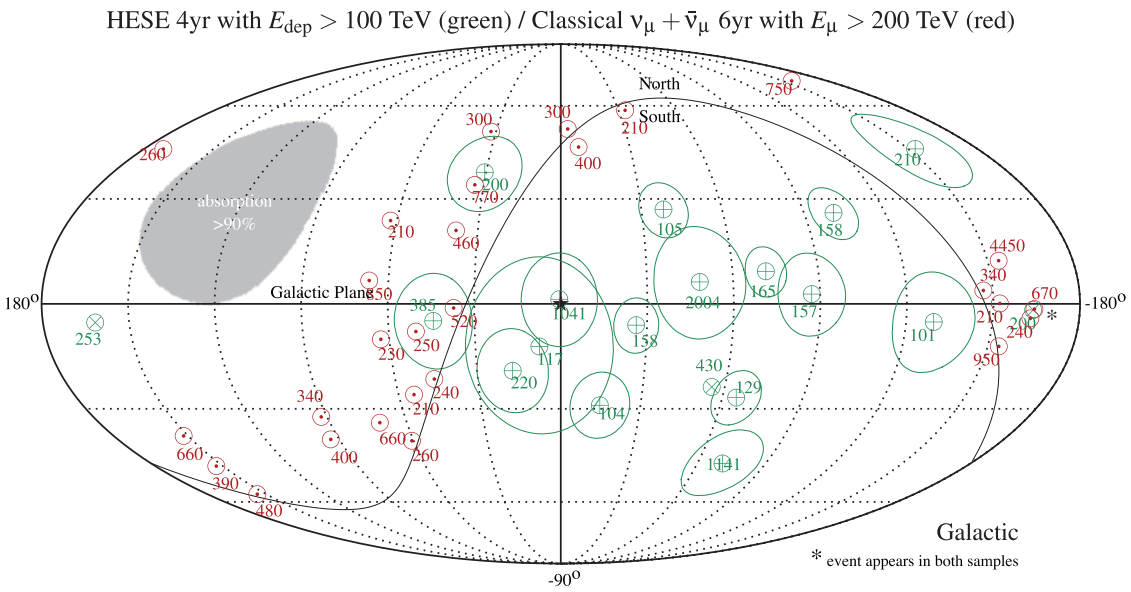

Fig. 6. Mollweide projection in Galactic coordinates of the arrival direction of neutrino events. We show the results of the six-year upgoing track analysis [6] with energy proxy MuEx > 50 ($\odot$). The red numbers show the most probable neutrino energy (in TeV) assuming the best-fit astrophysical flux of the analysis [6]. The events of the four-year high-energy starting event (HESE) analysis with deposited energy (green numbers) larger than 60 TeV (tracks $\otimes$ and cascades $\oplus$) are also shown [5,24]. Cascade events ($\oplus$) are indicated together with their median angular uncertainty (thin circles). One event (*) appears in both event samples. The gray-shaded region indicates the zenith angle range where Earth absorption of 100 TeV neutrinos is larger than 90%. The star symbol ($\star$) indicates the Galactic Center and the thin curved solid black line indicates the horizon.

energy suggests an excess of events in the 30–100 TeV energy range over and above a single power-law fit. This conclusion is supported by a subsequent analysis that has lowered the threshold of the starting-event analysis [19]. The astrophysical flux measured by IceCube is not featureless; either the spectrum of cosmic accelerators cannot be described by a single power law or a second component of cosmic neutrino sources emerges in the spectrum. The events are isolated neutrinos, and it is therefore very difficult to accommodate them as a feature in the atmospheric background, of charm origin or not [20]. The excess is already hinted at in the data shown in Fig. 1 and, in the context of that discussion, the energy associated with the photons that accompany the neutrino "excess" is not seen in the Fermi data [4]. This might indicate that the neutrinos originate in hidden sources [21] or in sources with a very strong cosmological evolution resulting in a shift of the photons to sub-GeV energies [22].

In Fig. 6 we show the arrival directions of the most energetic events of the six-year upgoing $\nu_\mu + \bar{\nu}_\mu$ analysis ($\odot$) and the four-year HESE analysis, separated into tracks ($\otimes$) and cascades ($\oplus$). The median angular resolution of the cascade events is indicated by thin circles around the best-fit position. The apparent anisotropy of the arrival directions is dominated by the effective area of the analysis. The most energetic muons with energy $E_\mu > 200$ TeV in the upgoing $\nu_\mu + \bar{\nu}_\mu$ analysis accumulate just below the horizon in the Northern Hemisphere due to Earth absorption. The HESE events with deposited energy of $E_{dep} > 100$ TeV also suffer from Earth absorption, but can also be visible in the Southern Hemisphere. Various analyses of the IceCube event distribution could not reveal a strong anisotropy from extended emission regions, which could indicate, e.g., a contribution from Galactic sources along the Galactic plane [23,24]. In fact, no correlation of the arrival directions

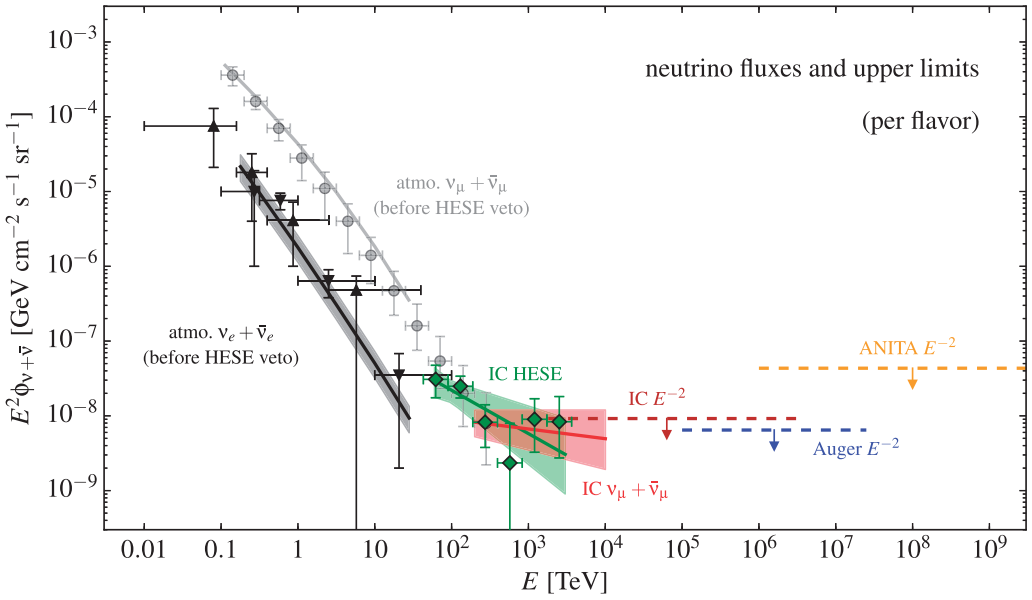

Fig. 7. Summary of neutrino observations and upper limits (per flavor). The black and gray data show IceCube's measurement of the atmospheric $\nu_e + \bar{\nu}_e$ [26,27] and $\nu_\mu + \bar{\nu}_\mu$ [28] spectra. The green data show the inferred bin-wise spectrum of the four-year high-energy starting event (HESE) analysis. The green line and green-shaded area indicate the best-fit and $1\,\sigma$ uncertainty range of a power-law fit to the HESE data. Note that the HESE analysis vetoes atmospheric neutrinos, and the true background level is much lower as indicated in the plot (cf. Fig. 5). In red we show the corresponding fit to the six-year $\nu_\mu + \bar{\nu}_\mu$ analysis. The dashed lines show 90% C.L. upper limits of an E^{-2} neutrino emission flux (dashed) at higher energies from IceCube [29] (brown), ANITA [30] (orange), and Auger [31] (blue).

of the highest-energy events, shown in Fig. 6, with potential sources or source classes has reached the level of $3\,\sigma$ [19].

Various scenarios have been invoked to explain the observed diffuse emission. The absence of strong anisotropies in the arrival direction of the data disfavors scenarios with strong Galactic emission. However, the limited event number and the low angular resolution of cascade-dominated samples can hide this type of emission. Scenarios that could have a partial contribution to the diffuse neutrino flux in the TeV–PeV energy range are the diffuse emission from Galactic CRs [32–37], the joint emission of Galactic CR sources [38–40], or very extended emission from the *Fermi bubbles* [32,41,42] or the Galactic halo [43,44]. More exotic scenarios consider dark matter decay [45–51] in the Galactic dark matter halo. A smoking gun of these local scenarios would be the observation of PeV gamma rays [32,52] that can only survive over Galactic distance scales.

On the other hand, an isotropic arrival direction of neutrinos is expected for extragalactic source populations. Various scenarios have been considered, including galaxies with intense star formation [4,53–59], cores of active galactic nuclei (AGNs) [60–62], low-luminosity AGNs [63,64], quasar-driven outflows [22], blazars [65–72], low-power gamma ray bursts (GRBs) [73–76], choked GRBs [77,78], cannonball GRBs [79], intergalactic shocks [80], galaxy clusters [4,81–83], tidal disruption events [84–87], or cosmogenic neutrinos [88,89].

An overview of the current information on the flux of cosmic neutrinos is shown in Fig. 7. As already mentioned, a challenge of most of these Galactic and extragalactic scenarios is the high intensity of the neutrino data at 10–100 TeV (see Fig. 7), which implies an equally high intensity of gamma rays produced via neutral pion production and decay. For extragalactic scenarios, this emission is

not directly visible due to the strong absorption in the extragalactic radiation background. However, this emission induces electromagnetic cascades that contribute strongly to the Fermi gamma ray background in the GeV–TeV range. We will discuss these multimessenger relations in the next section.

4. Multimessenger relations

Having established a prominent role for hadronic accelerators in the nonthermal universe, we investigate how the accelerated cosmic rays may produce photons and neutrinos after the relatively brief acceleration process. The principal mechanism at work is the production of pions in interactions of high-energy cosmic rays with photons or nuclei. Targets include strong radiation fields that may be associated with the accelerator as well as any concentrations of matter or molecular clouds in their vicinity. Finally, attenuation of the cosmic rays when propagating through the interstellar or intergalactic backgrounds can lead to further production of pions. A high-energy flux of neutrinos is then produced in the subsequent decay of charged pions via $\pi^+ \to \mu^+ + \nu_\mu$ followed by $\mu^+ \to e^+ + \nu_e + \bar{\nu}_\mu$ and the charge-conjugate processes. High-energy gamma rays are produced in the decay of neutral pions, $\pi^0 \to 2\gamma$.

Pion production of cosmic rays via scattering off photons can proceed resonantly via $p + \gamma \to \Delta^+ \to \pi^0 + p$ or $p + \gamma \to \Delta^+ \to \pi^+ + n$. These channels produce charged and neutral pions with probabilities of 2/3 and 1/3, respectively. However, the contribution of nonresonant pion production at the resonance changes this ratio to about 1/2 and 1/2. In contrast, cosmic rays interacting with hydrogen, e.g., in the Galactic disk, produce equal numbers of pions of all three charges in hadronic collisions: $p + p \to N_\pi\,[\,\pi^0 + \pi^+ + \pi^-] + X$, where N_π is the pion multiplicity.

To evaluate the flux of neutrinos from the cosmic ray interaction region, we start from the pion production rate $Q_{\pi^\pm}$, providing the number of charged pions per unit energy and time (units of $\mathrm{GeV}^{-1}\,\mathrm{s}^{-1}$). This quantity is proportional to the corresponding cosmic ray nucleon density Q_N by a "bolometric" proportionality factor $f_\pi \leq 1$ that parametrizes the efficiency of the conversion of cosmic ray energy into pion energy:

$$E_\pi^2 Q_{\pi^\pm}(E_\pi) \simeq f_\pi \frac{K_\pi}{1+K_\pi} \left[E_N^2 Q_N(E_N)\right]_{E_N = E_\pi/\kappa_\pi}. \tag{1}$$

The factor introducing K_π accounts for the different ratio between charged and neutral pions in interactions with gas or dust ("pp") and with radiation ("$p\gamma$"), with $K_\pi \simeq 2$ and 1, respectively. The total energy loss of the hadronic interaction (pp or $p\gamma$) is in the form of pions with average energy E_π, average multiplicity N_π, and *total* inelasticity κ. For $p\gamma$ interactions, the total inelasticity is about $\kappa \simeq 0.2$, whereas it is about $\kappa \simeq 0.5$ for pp interactions. In both cases the average inelasticity *per pion* can be approximated as $\kappa_\pi = \kappa/N_\pi \simeq 0.2$ [90]. The average energy per pion is then $E_\pi = \kappa_\pi E_N$. For a target with nucleon density n and diameter ℓ, the efficiency factor for producing pions can be expressed as

$$f_\pi = 1 - \exp(-\kappa \ell \sigma n), \tag{2}$$

with cross section σ and inelasticity κ for either $p\gamma$ or pp interactions.

Subsequently, the pions decay into gamma rays and neutrinos that carry, on average, 1/2 and 1/4 of the energy of the parent pion. We here make the approximation that, on average, the four leptons in the decay of $\pi^\pm$ equally share the charged pion's energy. The energy of the pionic leptons relative

to the proton is:

$$x_\nu = \frac{E_\nu}{E_p} = \frac{1}{4}\kappa_\pi \simeq \frac{1}{20} \text{ and } x_\gamma = \frac{E_\gamma}{E_p} = \frac{1}{2}\kappa_\pi \simeq \frac{1}{10}. \tag{3}$$

With this approximation, the neutrino production rate Q_{ν_α} can be related to the one for charged pions:

$$\frac{1}{3}\sum_\alpha E_\nu Q_{\nu_\alpha}(E_\nu) \simeq [E_\pi Q_{\pi^\pm}(E_\pi)]_{E_\pi \simeq 4E_\nu}\,. \tag{4}$$

Using Eqs. (1) and (4), we arrive at the final relation for neutrino production:

$$\frac{1}{3}\sum_\alpha E_\nu^2 Q_{\nu_\alpha}(E_\nu) \simeq \frac{1}{4} f_\pi \frac{K_\pi}{1+K_\pi}\left[E_N^2 Q_N(E_N)\right]_{E_N = 4E_\nu/\kappa_\pi}\,. \tag{5}$$

The production rate of gamma rays from the decay of neutral pions can be obtained in exactly the same way.

From the two equations for the productions of neutrinos and gamma rays, one can eliminate Q_N to obtain a model-independent relation that is independent of the details of the cosmic ray beam, except for the relative contribution of charged-to-neutral pions,

$$\frac{1}{3}\sum_\alpha E_\nu^2 Q_{\nu_\alpha}(E_\nu) \simeq \frac{K_\pi}{4}\left[E_\gamma^2 Q_\gamma(E_\gamma)\right]_{E_\gamma = 2E_\nu}\,. \tag{6}$$

Here, the prefactor $1/4$ accounts for the energy ratio $E_\nu/E_\gamma \simeq 1/2$ and the two gamma rays produced in the neutral pion decay. The relation simply reflects the fact that a π^0 produces two γ rays for every charged pion producing a $\nu_\mu + \bar{\nu}_\mu$ pair, which cannot be separated by current experiments. This is the simple counting that was used to derive the energy density in gamma rays in the universe accompanying the flux of cosmic neutrinos observed by IceCube, shown in Fig. 1.

5. Constraints on neutrino source populations

The failure of IceCube to identify sources in the diffuse cosmic neutrino flux [91] leads to constraints on the potential origin of these neutrinos. Individual neutrino sources at redshift z contribute a flux (units $\text{GeV}^{-1}\,\text{cm}^{-2}\,\text{s}^{-1}$ and summed over flavors)

$$\phi_\nu^{\text{PS}}(E_\nu) = \frac{(1+z)^2}{4\pi d_L^2(z)}\sum_\alpha Q_{\nu_\alpha}((1+z)E_\nu) \tag{7}$$

to the total diffuse flux, where d_L is the luminosity distance that, for a flat universe, is given by

$$d_L(z) = (1+z)\int_0^z \frac{dz'}{H(z')}, \tag{8}$$

with Hubble parameter H. For the standard ΛCDM cosmological model, the Hubble parameter scales as $H^2(z) = H_0^2[(1+z)^3\Omega_\text{m} + \Omega_\Lambda]$, with $\Omega_\text{m} \simeq 0.3$, $\Omega_\Lambda \simeq 0.7$, and $c/H_0 \simeq 4.4\,\text{Gpc}$ [92]. The diffuse neutrino flux from extragalactic sources is given by an integral over comoving volume

$\mathrm{d}V_c = 4\pi(d_L/(1+z))^2\mathrm{d}z/H(z)$, weighting each neutrino source by its density per comoving volume $\rho(z)$,

$$\phi_\nu(E_\nu) = \frac{c}{4\pi}\int_0^\infty \frac{dz}{H(z)}\rho(z)\sum_\alpha Q_{\nu_\alpha}((1+z)E_\nu). \tag{9}$$

In the following, we will assume that the neutrino emission rate Q_{ν_α} follows a power law $E^{-\Gamma}$. The flavor-averaged neutrino flux can then be written as

$$\frac{1}{3}\sum_\alpha E_\nu^2\phi_{\nu_\alpha}(E_\nu) = \frac{c}{4\pi}\frac{\xi_z}{H_0}\rho_0\frac{1}{3}\sum_\alpha E_\nu^2 Q_{\nu_\alpha}(E_\nu), \tag{10}$$

where we introduce the redshift factor

$$\xi_z = \int_0^\infty dz \frac{(1+z)^{-\Gamma}}{\sqrt{\Omega_\Lambda + (1+z)^3\Omega_\mathrm{m}}}\frac{\rho(z)}{\rho(0)}. \tag{11}$$

A spectral index of $\Gamma \simeq 2.0$ and no source evolution, $\rho(z) = \rho_0$, yields $\xi_z \simeq 0.6$, whereas the same spectral index and source evolution following the star formation rate yields $\rho \simeq 2.4$.

We can now investigate under what circumstances IceCube can detect the neutrino emission from individual, presumably nearby, point sources that contribute to the diffuse emission. Equation (10) relates the average luminosity of individual neutrino sources to the diffuse flux that is measured by the experiment to be $E^2\phi_\nu \simeq 10^{-8}\,\mathrm{GeV\,cm^{-2}\,s^{-1}\,sr^{-1}}$ for energies in excess of $\simeq 100\,\mathrm{TeV}$; see Fig. 7. From the measurement, we can infer the average emission from a single source [93]:

$$\frac{1}{3}\sum_\alpha E_\nu^2 Q_{\nu_\alpha}(E_\nu) \simeq 1.8\times 10^{43}\left(\frac{\xi_z}{2.4}\right)^{-1}\left(\frac{\rho_0}{10^{-8}\,\mathrm{Mpc^{-3}}}\right)^{-1}\mathrm{erg\,s^{-1}}. \tag{12}$$

For a homogenous distribution of sources, we expect, within the partial field of view f_sky of the full sky, one source within a distance d_1:

$$4\pi/3d_1^3\,\rho_0 f_\mathrm{sky} = 1. \tag{13}$$

Defining F_1 as the point source flux of a source with emission rate (12) at distance r_1, we can write down the probability distribution of the sources:

$$F\frac{dn}{dF} = \frac{3}{2}\left(\frac{F_1}{F}\right)^{\frac{3}{2}} e^{-\left(\frac{F_1}{F}\right)^{\frac{3}{2}}}. \tag{14}$$

The average flux from the closest source is then $\langle F\rangle \simeq 2.7F_1$, with median $F_\mathrm{med} \simeq 1.3F_1$. Assuming the latter as the emission of the closest source, we arrive at

$$\frac{1}{3}\sum_\alpha E_\nu^2\phi_{\nu_\alpha} \simeq 9\times 10^{-13}\left(\frac{f_\mathrm{sky}}{0.5}\right)^{\frac{2}{3}}\left(\frac{\xi_z}{2.4}\right)^{-1}\left(\frac{\rho_0}{10^{-8}\,\mathrm{Mpc^{-3}}}\right)^{-\frac{1}{3}}\mathrm{TeV\,cm^{-2}\,s^{-1}}. \tag{15}$$

Interestingly, this value is comparable to IceCube's point source sensitivity at the level of $5\times 10^{-13}\,\mathrm{TeV\,cm^{-2}\,s^{-1}}$ in the Northern Hemisphere [91].

In Fig. 8, we show the inferred local density and luminosity of neutrino source candidates from Ref. [94]. The gray-shaded region is excluded by nonobservation of sources as individual point sources, assuming the aforementioned sensitivity of IceCube in the Northern Hemisphere. The green

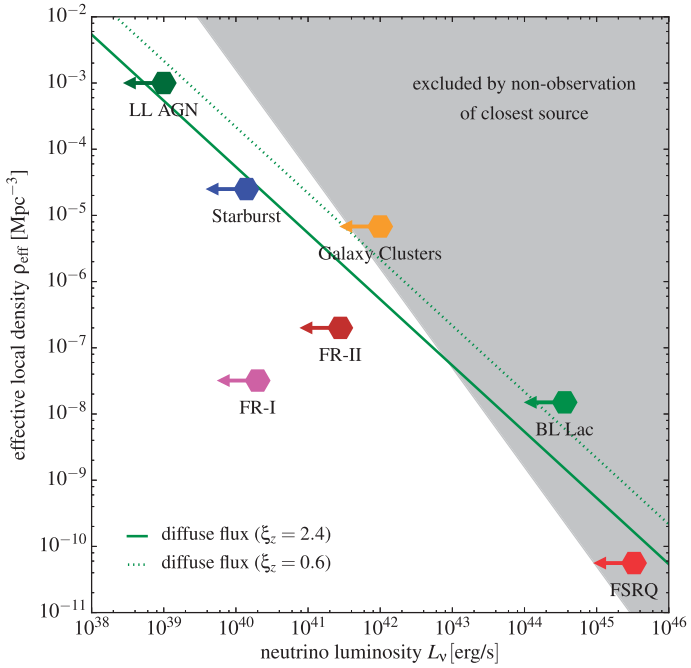

Fig. 8. The effective local density and (maximal) neutrino luminosity of various neutrino source candidates from Ref. [94]. The green solid (green dotted) line shows the local density and luminosity of the population of sources responsible for the diffuse neutrino flux of $E^2\phi \simeq 10^{-8}\,\mathrm{GeV\,cm^{-2}\,s^{-1}\,sr^{-1}}$ observed with IceCube, assuming source evolution following the star formation rate ($\xi_z \simeq 2.4$) or no source evolution ($\xi_z \simeq 0.6$), respectively. The gray-shaded area indicates source populations that are excluded by the nonobservation of point sources in the Northern Hemisphere ($f_{\rm sky} \simeq 0.5$) with sensitivity $E^2\phi^{\rm PS} \simeq 5 \times 10^{-13}\,\mathrm{TeV\,cm^{-2}\,s^{-1}}$.

lines show the combination of density and luminosity for sources at the level of the observed IceCube flux, assuming a source density evolution following the star formation rate (solid line) or no evolution (dotted line). We conclude that IceCube is presently sensitive to source populations with local source densities lower than about $6 \times 10^{-8}\,\mathrm{Mpc^{-3}}$, and much lower local densities, like flat spectrum radio quasars, are excluded by the nonobservation of individual sources. Some source classes, like Fanaroff–Riley (FR) radio galaxies, have an estimated neutrino luminosity that is too low for the observed flux. Note that these estimates depend on the evolution parameter ξ_z, and the exact sensitivity estimate depends on the particular redshift evolution of the source luminosity density. In addition, this simple estimate can be refined by considering not only the closest source of the population but the combined emission of *known* local sources; see, e.g., Ref. [93].

6. The energy density of extragalactic cosmic rays

Is it possible that the sources of the extragalactic cosmic rays are themselves neutrino sources? From the measured cosmic ray spectrum, one can derive that the emission rate density of nucleons is at the level of [95,96]

$$\mathcal{L}_N = \rho_0 E_N^2 Q_N(E_p) \simeq (1-2) \times 10^{44}\,\mathrm{erg\,Mpc^{-3}\,yr^{-1}}. \tag{16}$$

Combining this with Eq. (5), we can derive the diffuse neutrino flux:

$$\frac{1}{3}\sum_\alpha E_\nu^2 \phi_{\nu_\alpha}(E_\nu) \simeq f_\pi \frac{\xi_z K_\pi}{1+K_\pi}(2-4) \times 10^{-8}\,\mathrm{GeV\,cm^{-2}\,s^{-1}\,sr^{-1}}. \tag{17}$$

Here, ξ_z is the evolution factor previously introduced. The requirement $f_\pi \leq 1$ limits the neutrino production by the actual sources of the cosmic rays as pointed out in the seminal work by Waxman and Bahcall [12]. For optically thin sources, $f_\pi \ll 1$, neutrino production is only a small by-product of the acceleration process. The energy loss associated with pion production must not limit the sources' ability to accelerate the cosmic rays. On the other hand, optically thick sources, $f_\pi \simeq 1$, may be efficient neutrino emitters. Realistic sources of this type need different zones, one zone for the acceleration process ($f_\pi \ll 1$) and a second zone for the efficient conversion of cosmic rays to neutrinos ($f_\pi \simeq 1$). Examples of this scenario are sources embedded in starburst galaxies, where cosmic rays can be stored over sufficiently long timescales to yield significant neutrino production.

For $\xi_z \simeq 2.4$ and $K_\pi \simeq 1$–2, the upper bound resulting from Eq. (17) and $f_\pi = 1$ is at the level of the neutrino flux observed by IceCube. Therefore, it is possible that the observed extragalactic cosmic rays and neutrinos have the same origin. A plausible scenario is a "calorimeter" in which only cosmic rays with energy below a few 10 PeV interact efficiently. An energy dependence of the calorimetric environment can be introduced by energy-dependent diffusion. If $D(E)$ is the diffusion coefficient, then the timescale of escape from the calorimeter is given by the solution to $6D(E)t = d^2$, where d is the effective size of the region. Typically, we have $D(E) \propto E^\delta$ with $\delta \simeq 0.3$–0.6. In the following, we again consider the case of protons. Taking $\sigma_{pp} \simeq 8 \times 10^{-26}\,\mathrm{cm}^2$ at $E_p = 100\,\mathrm{PeV}$ and the diffusion coefficient of $D(E_p) \simeq D_{\mathrm{GeV}}(E_p/1\,\mathrm{GeV})^{1/3}$, the pp thickness can be expressed as $\tau_{pp} \simeq ctn_{\mathrm{gas}}\sigma_{pp}$, or

$$\tau_{pp} \simeq 0.18 \left(\frac{d}{100\,\mathrm{pc}}\right)^2 \left(\frac{D_{\mathrm{GeV}}}{10^{26}\,\mathrm{cm}^2\,\mathrm{s}^{-1}}\right)^{-1} \left(\frac{E_p}{10\,\mathrm{PeV}}\right)^{-1/3} \left(\frac{n}{100\,\mathrm{cm}^{-3}}\right). \tag{18}$$

Here, we have used feasible parameters of starburst galaxies [4,53]. Therefore, depending on the calorimetric environment, it is possible that the flux below a few PeV is efficiently converted to neutrinos and contributes to the TeV–PeV diffuse emission observed by IceCube.

7. Cosmogenic neutrinos

The production of neutrinos in the sources that accelerate the high-energy cosmic rays depends on the source environment. In order to efficiently accelerate cosmic rays, any loss mechanism, including pion production in $p\gamma$ and pp interactions, must be suppressed as it reduces the acceleration time. Efficient accelerators are likely to be inefficient beam dumps for producing neutrinos. High-efficiency neutrino production can be achieved by separating the sites of acceleration and neutrino production. For instance, after acceleration, extragalactic cosmic rays propagate over cosmological distances of more than 10 Mpc and can efficiently produce neutrinos on the dilute extragalactic medium.

In this section, we will discuss the production of neutrinos in the interactions of extragalactic cosmic rays with cosmic radiation backgrounds. Soon after the discovery of the cosmic microwave background (CMB), Greisen, Zatsepin, and Kuzmin [97,98] (GZK) realized that extragalactic cosmic rays are attenuated by interactions with background photons. Actually, protons interact resonantly via $p\gamma \to \Delta^+ \to \pi^+ n$ with background photons with mean energy $\epsilon \simeq 0.33\,\mathrm{meV}$ at energies $E_p \simeq (m_\Delta^2 - m_p^2)/4/\epsilon \simeq 500\,\mathrm{EeV}$. The width of the Planck spectrum leads to a significant attenuation of proton fluxes after propagation over distances on the order of 200 Mpc at an energy above $E_{\mathrm{GZK}} \simeq 50\,\mathrm{EeV}$, which is known as GZK suppression. Also, heavier nuclei are attenuated at a similar energy by photodisintegration of the nucleus by CMB photons via the giant dipole resonance.

The pions produced in GZK interactions decay, resulting in a detectable flux of *cosmogenic* neutrinos first estimated by Berezinsky and Zatsepin [99] in 1969. This *guaranteed* flux of neutrinos

became one of the benchmarks for high-energy neutrino astronomy leading early on to the concept of kilometer-scale detectors. The flux of cosmogenic neutrinos peaks at EeV neutrino energy depending on the chemical composition and the evolution with redshift of the unknown sources. The largest neutrino flux results from proton-dominated models [100–102]. A particularly strong emission can be expected in such models if the proton spectrum extends below the ankle. Referred to as "dip models," the ankle results from the absorption of protons by Bethe–Heitler pair production on CMB photons. A fit to the observed cosmic ray spectrum requires relative strong source evolution with redshift [103–106] that enhances pion production. However, the corresponding electromagnetic emission via neutral pions as well as $e^{\pm}$ pairs is constrained by the isotropic gamma ray background (IGRB) observed by Fermi LAT [107,108] and limits the neutrino intensity of these proton-dominated scenarios [109–114]. Recent upper limits on cosmogenic neutrinos resulting from the failure by IceCube to observe EeV neutrinos constrains proton-dominated models [29].

In contrast, the IceCube constraint can be accommodated by introducing a heavy nuclear composition. Resonant neutrino production still proceeds via the interaction of individual nucleons with background photons, but the threshold of the production is increased to $E_{\rm CR} \gtrsim AE_{\rm GZK}$ for nuclei with mass number A. Therefore, efficient cosmogenic neutrino production would require an injected cosmic ray flux that extends well above $E_{\rm GZK}$. Especially for heavier nuclear composition of the primary flux, the production of neutrinos on photons of the extragalactic background light (EBL) becomes relatively important [95,112,115–122]. The interaction with optical photons produces neutrino fluxes in the PeV energy range. However, the overall level is much lower because of the low intensity of the EBL photons. It is unlikely that the PeV neutrino flux observed with IceCube could be related to the neutrino production in the EBL [88] (see also Ref. [89]). The observed PeV neutrino flux level is too high to be consistent with associated electromagnetic contributions to the IGRB or upper limits on the EeV neutrino flux.

8. Correlation with UHE CR events

Cosmic rays above the GZK cutoff have an absorption length on the order of 200 Mpc. Therefore, the observed events have to originate in the local universe. In combination with the high rigidity, $\mathcal{R} \propto E/Z$, of these events, the deflection in extragalactic and Galactic magnetic fields can be low enough to find anisotropies in the UHE CR arrival direction. Figure 9 shows the distribution of events observed with Auger [123] above 52 EeV ($\times$) and Telescope Array [124] above 57 EeV ($+$). To highlight feasible anisotropies in the arrival direction of the combined data set, we smooth the events at best-fit position $\mathbf{n}_i$ over the sphere with unit vector $\mathbf{n}$ following a von Mises–Fisher distribution, $f_i(\mathbf{n}) = a \exp(a\mathbf{n}\cdot\mathbf{n}_i)/\sinh a/(4\pi)$. The parameter a is fixed to 11.5 such that 50% of the distribution is contained within an opening angle of 20°. From the smoothed event distribution $f(\mathbf{n}) = \sum_i f_i(\mathbf{n})$, we define $\bar{f}(\delta)$ as the average of the distribution f in each declination bin δ and define the anisotropy as

$$\delta I(\mathbf{n}) = f(\mathbf{n})/\bar{f}(\delta(\mathbf{n})) - 1. \tag{19}$$

This simple procedure ensures that spurious anisotropies coming from the detector exposures that depend mostly on declination are corrected from the map. The anisotropy map recovers two small-scale excess regions in the Northern and Southern Hemisphere that coincide with the excess regions reported by Telescope Array [124] (sampling radius of 20°; post-trial p-value of 3.7×10^{-4}) and

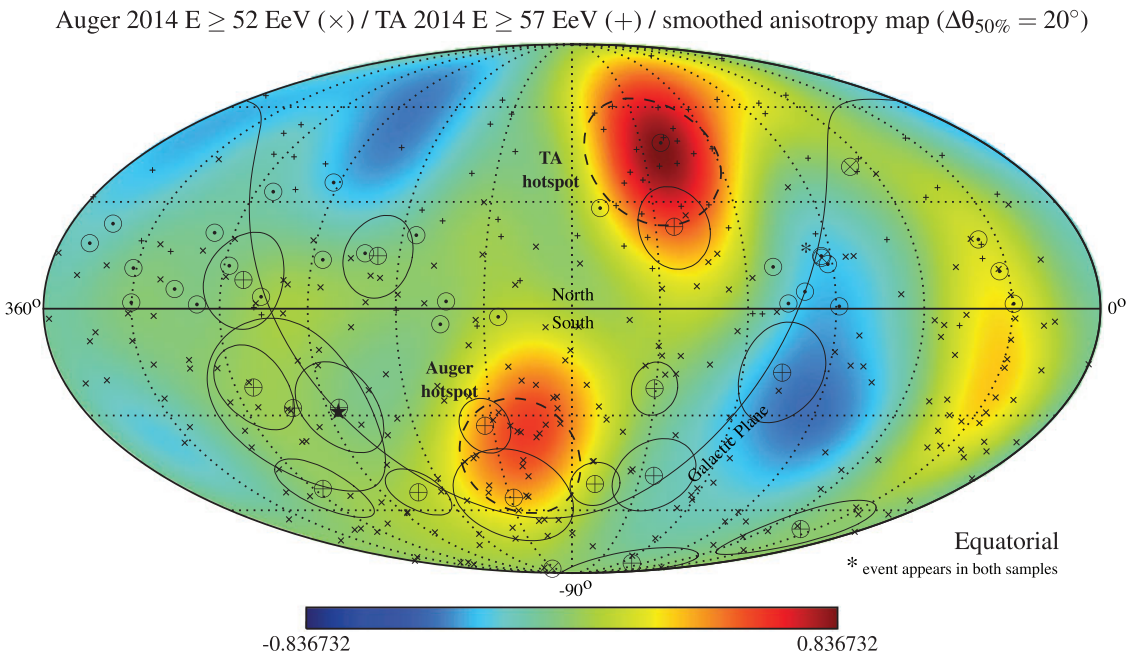

Fig. 9. Mollweide projection of the arrival direction of neutrinos and UHE CRs. The neutrino sample is identical to the one shown in Fig. 6. We show events from Auger [123] above 54 EeV (×) and from Telescope Array [124] above 57 EeV (+). The background shows the anisotropy of the combined UHE CR map derived with the method described in the main text and smoothed with with $\theta_{50\%} = 20^\circ$. We highlight the excess regions found by Auger (sampling radius of 15°; post-trial p-value of 1.4×10^{-2}) and Telescope Array (sampling radius of 20°; post-trial p-value of 3.7×10^{-4}).

Auger [123] in the direction of Centaurus A (sampling radius of 15°; post-trial p-value of 1.4×10^{-2}), respectively. These are indicated as dashed circles of different sizes.

Figure 9 also shows the same neutrino event candidates that were shown in Fig. 6. It is apparent that there is no noticeable clustering of high-energy neutrino events in the direction of these hot spots. Indeed, a dedicated analysis [125] by Telescope Array, Auger, and IceCube did not identify significant cross-correlation of neutrino and UHE CR events (below $3.3\,\sigma$). However, this does not necessarily rule out the possibility that the events emerge from the same sources. Neutrino events can be observed from all UHE CR sources up to the Hubble horizon $c/H_0 \simeq 4.4$ Gpc. On the other hand, UHE CRs above the energy shown in Fig. 9 have to emerge from local sources up to 200 Mpc. Therefore, we can estimate that only a fraction of 200 Mpc/4.4 Gpc $\simeq$ 5% of astrophysical neutrinos should correlate with UHE CRs. The total number of neutrino events shown in Fig. 9 is only 45, so maybe two events are expected to correlate with the anisotropy structure suggested by UHE CRs.

9. Conclusions

IceCube has discovered a flux of extragalactic cosmic neutrinos with an energy density that matches that of extragalactic high-energy photons and ultra-high-energy cosmic rays. This may suggest that neutrinos and high-energy cosmic rays share a common origin. They may originate in calorimetric environments like starburst galaxies or galaxy clusters hosting the cosmic ray accelerators. Identification of the sources by observation of multiple neutrino events from these sources with IceCube will be challenging. However, the possibility exists for revealing the sources by the comprehensive IceCube multimessenger program.

Further progress requires larger instruments. We therefore propose as a next step the extraordinary opportunity of instrumenting $10\,\mathrm{km}^3$ of glacial ice at the South Pole and thereby improving on IceCube's sensitive volume by an order of magnitude [126]. This large gain is made possible by the unique optical properties of the Antarctic glacier revealed by the construction of IceCube. As a consequence of the extremely long photon absorption lengths in the deep Antarctic ice, the spacing between strings of light sensors can be increased from 125 m to over 250 m without loss of performance of the instrument. The instrumented volume can therefore grow by one order of magnitude while keeping the construction budget of a next-generation instrument at the level of the cost of the current IceCube detector. The new facility will increase the event rates of cosmic events from hundreds to thousands over several years.

Acknowledgements

Discussion with collaborators inside and outside the IceCube Collaboration, too many to be listed, have greatly shaped this presentation. Thanks. This research was supported in part by the U.S. National Science Foundation under grants PLR-1600823 and PHY-1607644, and by the University of Wisconsin Research Committee with funds granted by the Wisconsin Alumni Research Foundation.

References

[1] M. G. Aartsen et al., arXiv:1612.05093 [astro-ph.IM] [Search INSPIRE].
[2] M. Ahlers and F. Halzen, Rept. Prog. Phys. **78**, 126901 (2015).
[3] B. P. Abbott et al., Phys. Rev. Lett. **116**, 131103 (2016) [arXiv:1602.03838 [gr-qc]] [Search INSPIRE].
[4] K. Murase, M. Ahlers, and B. C. Lacki, Phys. Rev. D **88**, 121301 (2013) [arXiv:1306.3417 [astro-ph.HE]] [Search INSPIRE].
[5] M. G. Aartsen et al., Phys. Rev. Lett. **113**, 101101 (2014) [arXiv:1405.5303 [astro-ph.HE]] [Search INSPIRE].
[6] M. G. Aartsen et al., Astrophys. J. **833**, 3 (2016) [arXiv:1607.08006 [astro-ph.HE]] [Search INSPIRE].
[7] M. G. Aartsen et al., JINST **11**, P11009 (2016) [arXiv:1610.01814 [hep-ex]] [Search INSPIRE].
[8] M. G. Aartsen et al., arXiv:1612.06028 [astro-ph.HE] [Search INSPIRE].
[9] S. Schonert, T. K. Gaisser, E. Resconi, and O. Schulz, Phys. Rev. D **79**, 043009 (2009) [arXiv:0812.4308 [astro-ph]] [Search INSPIRE].
[10] J. Ahrens et al. [AMANDA Collaboration], Nucl. Instrum. Meth. A **524**, 169 (2004) [arXiv:astro-ph/0407044] [Search INSPIRE].
[11] M. G. Aartsen et al., JINST **9**, P03009 (2014) [arXiv:1311.4767 [physics.ins-det]] [Search INSPIRE].
[12] E. Waxman and J. N. Bahcall, Phys. Rev. D **59**, 023002 (1999) [arXiv:hep-ph/9807282] [Search INSPIRE].
[13] J. N. Bahcall and E. Waxman, Phys. Rev. D **64**, 023002 (2001) [arXiv:hep-ph/9902383] [Search INSPIRE].
[14] M. G. Aartsen et al., Phys. Rev. Lett. **115**, 081102 (2015) [arXiv:1507.04005 [astro-ph.HE]] [Search INSPIRE].
[15] M. G. Aartsen et al., Phys. Rev. Lett. **111**, 021103 (2013) [arXiv:1304.5356 [astro-ph.HE]] [Search INSPIRE].
[16] M. G. Aartsen et al., Science **342**, 1242856 (2013) [arXiv:1311.5238 [astro-ph.HE]] [Search INSPIRE].
[17] T. K. Gaisser, K. Jero, A. Karle, and J. van Santen, Phys. Rev. D **90**, 023009 (2014) [arXiv:1405.0525 [astro-ph.HE]] [Search INSPIRE].
[18] M. G. Aartsen et al., Phys. Rev. Lett. **114**, 171102 (2015) [arXiv:1502.03376 [astro-ph.HE]] [Search INSPIRE].
[19] M. G. Aartsen et al., Astrophys. J. **824**, L28 (2016) [arXiv:1605.00163 [astro-ph.HE]] [Search INSPIRE].
[20] F. Halzen and L. Wille, Phys. Rev. D **94**, 014014 (2016) [arXiv:1605.01409 [hep-ph]] [Search INSPIRE].

[21] K. Murase, D. Guetta, and M. Ahlers, Phys. Rev. Lett. **116**, 071101 (2016) [arXiv:1509.00805 [astro-ph.HE]] [Search INSPIRE].
[22] X. Wang and A. Loeb, J. Cosmol. Astropart. Phys. **1612**, 012 (2016) [arXiv:1607.06476 [astro-ph.HE]] [Search INSPIRE].
[23] M. Ahlers, Y. Bai, V. Barger, and R. Lu, Phys. Rev. D **93**, 013009 (2016) [arXiv:1505.03156 [hep-ph]] [Search INSPIRE].
[24] M. G. Aartsen et al., Proc. 34th Int. Cosmic Ray Conf. (ICRC 2015) (2015) [arXiv:1510.05223 [astro-ph.HE]] [Search INSPIRE].
[25] M. G. Aartsen et al., Phys. Rev. D **89**, 102001 (2014) [arXiv:1312.0104 [astro-ph.HE]] [Search INSPIRE].
[26] M. G. Aartsen et al., Phys. Rev. Lett. **110**, 151105 (2013) [arXiv:1212.4760 [hep-ex]] [Search INSPIRE].
[27] M. G. Aartsen et al., Phys. Rev. D **91**, 122004 (2015) [arXiv:1504.03753 [astro-ph.HE]] [Search INSPIRE].
[28] R. Abbasi et al., Phys. Rev. D **83**, 012001 (2011) [arXiv:1010.3980 [astro-ph.HE]] [Search INSPIRE].
[29] M. G. Aartsen et al., Phys. Rev. Lett. **117**, 241101 (2016) [arXiv:1607.05886 [astro-ph.HE]] [Search INSPIRE].
[30] P. W. Gorham et al., Phys. Rev. D **82**, 022004 (2010); **85**, 049901 (2012) [erratum] [arXiv:1011.5004 [astro-ph.HE]] [Search INSPIRE].
[31] A. Aab et al., Phys. Rev. D **91**, 092008 (2015) [arXiv:1504.05397 [astro-ph.HE]] [Search INSPIRE].
[32] M. Ahlers and K. Murase, Phys. Rev. D **90**, 023010 (2014) [arXiv:1309.4077 [astro-ph.HE]] [Search INSPIRE].
[33] J. C. Joshi, W. Winter, and N. Gupta, Mon. Not. Roy. Astron. Soc. **439**, 3414 (2014); **446**, 892 (2014) [erratum] [arXiv:1310.5123 [astro-ph.HE]] [Search INSPIRE].
[34] A. Neronov, D. V. Semikoz, and C. Tchernin, Phys. Rev. D **89**, 103002 (2014) [arXiv:1307.2158 [astro-ph.HE]] [Search INSPIRE].
[35] M. Kachelriess and S. Ostapchenko, Phys. Rev. D **90**, 083002 (2014) [arXiv:1405.3797 [astro-ph.HE]] [Search INSPIRE].
[36] D. Gaggero, D. Grasso, A. Marinelli, A. Urbano, and M. Valli, Astrophys. J. **815**, L25 (2015) [arXiv:1504.00227 [astro-ph.HE]] [Search INSPIRE].
[37] A. Neronov and D. V. Semikoz, Astropart. Phys. **75**, 60 (2016) [arXiv:1509.03522 [astro-ph.HE]] [Search INSPIRE].
[38] D. B. Fox, K. Kashiyama, and P. Mészáros, Astrophys. J. **774**, 74 (2013) [arXiv:1305.6606 [astro-ph.HE]] [Search INSPIRE].
[39] M. C. Gonzalez-Garcia, F. Halzen, and V. Niro, Astropart. Phys. **57–58**, 39 (2014) [arXiv:1310.7194 [astro-ph.HE]] [Search INSPIRE].
[40] L. A. Anchordoqui, H. Goldberg, T. C. Paul, L. H. M. da Silva, and B. J. Vlcek, Phys. Rev. D **90**, 123010 (2014) [arXiv:1410.0348 [astro-ph.HE]] [Search INSPIRE].
[41] S. Razzaque, Phys. Rev. D **88**, 081302 (2013) [arXiv:1309.2756 [astro-ph.HE]] [Search INSPIRE].
[42] C. Lunardini, S. Razzaque, K. T. Theodoseau, and L. Yang, Phys. Rev. D **90**, 023016 (2014) [arXiv:1311.7188 [astro-ph.HE]] [Search INSPIRE].
[43] A. M. Taylor, S. Gabici, and F. Aharonian, Phys. Rev. D **89**, 103003 (2014) [arXiv:1403.3206 [astro-ph.HE]] [Search INSPIRE].
[44] O. Kalashev and S. Troitsky, Phys. Rev. D **94**, 063013 (2016) [arXiv:1608.07421 [astro-ph.HE]] [Search INSPIRE].
[45] B. Feldstein, A. Kusenko, S. Matsumoto, and T. T. Yanagida, Phys. Rev. D **88**, 015004 (2013) [arXiv:1303.7320 [hep-ph]] [Search INSPIRE].
[46] A. Esmaili and P. D. Serpico, J. Cosmol. Astropart. Phys. **1311**, 054 (2013) [arXiv:1308.1105 [hep-ph]] [Search INSPIRE].
[47] Y. Bai, R. Lu, and J. Salvado, J. High Energy Phys. **01**, 161 (2016) [arXiv:1311.5864 [hep-ph]] [Search INSPIRE].
[48] K. Murase, R. Laha, S. Ando, and M. Ahlers, Phys. Rev. Lett. **115**, 071301 (2015) [arXiv:1503.04663 [hep-ph]] [Search INSPIRE].
[49] S. M. Boucenna, M. Chianese, G. Mangano, G. Miele, S. Morisi, O. Pisanti, and E. Vitagliano, J. Cosmol. Astropart. Phys. **1512**, 055 (2015) [arXiv:1507.01000 [hep-ph]] [Search INSPIRE].

[50] M. Chianese, G. Miele, and S. Morisi, J. Cosmol. Astropart. Phys. **1701**, 007 (2017) [arXiv:1610.04612 [hep-ph]] [Search INSPIRE].
[51] T. Cohen, K. Murase, N. L. Rodd, B. R. Safdi, and Y. Soreq, arXiv:1612.05638 [hep-ph] [Search INSPIRE].
[52] N. Gupta, Astropart. Phys. **48**, 75 (2013) [arXiv:1305.4123 [astro-ph.HE]] [Search INSPIRE].
[53] A. Loeb and E. Waxman, J. Cosmol. Astropart. Phys. **0605**, 003 (2006) [arXiv:astro-ph/0601695] [Search INSPIRE].
[54] H. -N. He, T. Wang, Y. -Z. Fan, S. -M. Liu, and D. -M. Wei, Phys. Rev. D **87**, 063011 (2013) [arXiv:1303.1253 [astro-ph.HE]] [Search INSPIRE].
[55] L. A. Anchordoqui, T. C. Paul, L. H. M. da Silva, D. F. Torres, and B. J. Vlcek, Phys. Rev. D **89**, 127304 (2014) [arXiv:1405.7648 [astro-ph.HE]] [Search INSPIRE].
[56] X. -C. Chang and X. -Y. Wang, Astrophys. J. **793**, 131 (2014) [arXiv:1406.1099 [astro-ph.HE]] [Search INSPIRE].
[57] I. Tamborra, S. Ando, and K. Murase, J. Cosmol. Astropart. Phys. **1409**, 043 (2014) [arXiv:1404.1189 [astro-ph.HE]] [Search INSPIRE].
[58] K. Bechtol, M. Ahlers, M. Di Mauro, M. Ajello, and J. Vandenbroucke, arXiv:1511.00688 [astro-ph.HE] [Search INSPIRE].
[59] N. Senno, P. Mészáros, K. Murase, P. Baerwald, and M. J. Rees, Astrophys. J. **806**, 24 (2015) [arXiv:1501.04934 [astro-ph.HE]] [Search INSPIRE].
[60] F. W. Stecker, C. Done, M. H. Salamon, and P. Sommers, Phys. Rev. Lett. **66**, 2697 (1991).
[61] F. W. Stecker, Phys. Rev. D **88**, 047301 (2013) [arXiv:1305.7404 [astro-ph.HE]] [Search INSPIRE].
[62] O. Kalashev, D. Semikoz, and I. Tkachev, J. Exp. Theor. Phys. **120**, 541 (2015) [arXiv:1410.8124 [astro-ph.HE]] [Search INSPIRE].
[63] Y. Bai, A. J. Barger, V. Barger, R. Lu, A. D. Peterson, and J. Salvado, Phys. Rev. D **90**, 063012 (2014) [arXiv:1407.2243 [astro-ph.HE]] [Search INSPIRE].
[64] S. S. Kimura, K. Murase, and K. Toma, Astrophys. J. **806**, 159 (2015) [arXiv:1411.3588 [astro-ph.HE]] [Search INSPIRE].
[65] F. Tavecchio and G. Ghisellini, Mon. Not. Roy. Astron. Soc. **451**, 1502 (2015) [arXiv:1411.2783 [astro-ph.HE]] [Search INSPIRE].
[66] P. Padovani and E. Resconi, Mon. Not. Roy. Astron. Soc. **443**, 474 (2014) [arXiv:1406.0376 [astro-ph.HE]] [Search INSPIRE].
[67] C. D. Dermer, K. Murase, and Y. Inoue, J. High Energy Astrophys. **3–4**, 29 (2014) [arXiv:1406.2633 [astro-ph.HE]] [Search INSPIRE].
[68] M. Petropoulou, S. Dimitrakoudis, P. Padovani, A. Mastichiadis, and E. Resconi, Mon. Not. Roy. Astron. Soc. **448**, 2412 (2015) [arXiv:1501.07115 [astro-ph.HE]] [Search INSPIRE].
[69] P. Padovani, M. Petropoulou, P. Giommi, and E. Resconi, Mon. Not. Roy. Astron. Soc. **452**, 1877 (2015) [arXiv:1506.09135 [astro-ph.HE]] [Search INSPIRE].
[70] M. Kadler et al., Nature Phys. **12**, 807 (2016) [arXiv:1602.02012 [astro-ph.HE]] [Search INSPIRE].
[71] P. Padovani, E. Resconi, P. Giommi, B. Arsioli, and Y. L. Chang, Mon. Not. Roy. Astron. Soc. **457**, 3582 (2016) [arXiv:1601.06550 [astro-ph.HE]] [Search INSPIRE].
[72] A. Neronov, D. V. Semikoz, and K. Ptitsyna, arXiv:1611.06338 [astro-ph.HE] [Search INSPIRE].
[73] E. Waxman and J. N. Bahcall, Phys. Rev. Lett. **78**, 2292 (1997) [arXiv:astro-ph/9701231] [Search INSPIRE].
[74] S. Ando and J. F. Beacom, Phys. Rev. Lett. **95**, 061103 (2005) [arXiv:astro-ph/0502521] [Search INSPIRE].
[75] K. Murase and K. Ioka, Phys. Rev. Lett. **111**, 121102 (2013) [arXiv:1306.2274 [astro-ph.HE]] [Search INSPIRE].
[76] I. Tamborra and S. Ando, Phys. Rev. D **93**, 053010 (2016) [arXiv:1512.01559 [astro-ph.HE]] [Search INSPIRE].
[77] P. Meszaros and E. Waxman, Phys. Rev. Lett. **87**, 171102 (2001) [arXiv:astro-ph/0103275] [Search INSPIRE].
[78] N. Senno, K. Murase, and P. Meszaros, Phys. Rev. D **93**, 083003 (2016) [arXiv:1512.08513 [astro-ph.HE]] [Search INSPIRE].
[79] S. Dado and A. Dar, Phys. Rev. Lett. **113**, 191102 (2014) [arXiv:1405.5487 [astro-ph.HE]] [Search INSPIRE].

[80] K. Kashiyama and P. Mészáros, Astrophys. J. **790**, L14 (2014) [arXiv:1405.3262 [astro-ph.HE]] [Search INSPIRE].
[81] V. S. Berezinsky, P. Blasi, and V. S. Ptuskin, Astrophys J. **487**, 529 (1997) [arXiv:astro-ph/9609048] [Search INSPIRE].
[82] K. Murase, S. Inoue, and S. Nagataki, Astrophys. J. **689**, L105 (2008) [arXiv:0805.0104 [astro-ph]] [Search INSPIRE].
[83] F. Zandanel, I. Tamborra, S. Gabici, and S. Ando, Astron. Astrophys. **578**, A32 (2015) [arXiv:1410.8697 [astro-ph.HE]] [Search INSPIRE].
[84] X. -Yu Wang and R. -Yu Liu, Phys. Rev. D **93**, 083005 (2016) [arXiv:1512.08596 [astro-ph.HE]] [Search INSPIRE].
[85] N. Senno, K. Murase, and P. Meszaros, arXiv:1612.00918 [astro-ph.HE] [Search INSPIRE].
[86] L. Dai and K. Fang, arXiv:1612.00011 [astro-ph.HE] [Search INSPIRE].
[87] C. Lunardini and W. Winter, arXiv:1612.03160 [astro-ph.HE] [Search INSPIRE].
[88] E. Roulet, G. Sigl, A. van Vliet, and S. Mollerach, J. Cosmol. Astropart. Phys. **1301**, 028 (2013) [arXiv:1209.4033 [astro-ph.HE]] [Search INSPIRE].
[89] L. Yacobi, D. Guetta, and E. Behar, Astrophys. J. **823**, 89 (2016) [arXiv:1510.01244 [astro-ph.HE]] [Search INSPIRE].
[90] S. R. Kelner, F. A. Aharonian, and V. V. Bugayov, Phys. Rev. D **74**, 034018, (2006); **79**, 039901 (2009) [erratum] [arXiv:astro-ph/0606058] [Search INSPIRE].
[91] M. G. Aartsen et al., arXiv:1609.04981 [astro-ph.HE] [Search INSPIRE].
[92] C. Patrignani et al., Chin. Phys. C **40**, 100001 (2016).
[93] M. Ahlers and F. Halzen, Phys. Rev. D **90**, 043005 (2014) [arXiv:1406.2160 [astro-ph.HE]] [Search INSPIRE].
[94] P. Mertsch, M. Rameez, and I. Tamborra, arXiv:1612.07311 [astro-ph.HE] [Search INSPIRE].
[95] M. Ahlers and F. Halzen, Phys. Rev. D **86**, 083010 (2012) [arXiv:1208.4181 [astro-ph.HE]] [Search INSPIRE].
[96] B. Katz, E. Waxman, T. Thompson, and A. Loeb, arXiv:1311.0287 [astro-ph.HE] [Search INSPIRE].
[97] K. Greisen, Phys. Rev. Lett. **16**, 748 (1966).
[98] G. T. Zatsepin and V. A. Kuzmin, JETP Lett. **4**, 78 (1966).
[99] V. S. Berezinsky and G. T. Zatsepin, Phys. Lett. B **28**, 423 (1969).
[100] S. Yoshida and M. Teshima, Prog. Theor. Phys. **89**, 833 (1993).
[101] R. J. Protheroe and P. A. Johnson, Astropart. Phys. **4**, 253 (1996) [arXiv:astro-ph/9506119] [Search INSPIRE].
[102] R. Engel, D. Seckel, and T. Stanev, Phys. Rev. D **64**, 093010 (2001) [arXiv:astro-ph/0101216] [Search INSPIRE].
[103] V. Berezinsky, A. Z. Gazizov, and S. I. Grigorieva, Phys. Rev. D **74**, 043005 (2006) [arXiv:hep-ph/0204357] [Search INSPIRE].
[104] Z. Fodor, S. D. Katz, A. Ringwald, and H. Tu, J. Cosmol. Astropart. Phys. **0311**, 015 (2003) [arXiv:hep-ph/0309171] [Search INSPIRE].
[105] H. Yuksel and M. D. Kistler, Phys. Rev. D **75**, 083004 (2007) [arXiv:astro-ph/0610481] [Search INSPIRE].
[106] H. Takami, K. Murase, S. Nagataki, and K. Sato, Astropart. Phys. **31**, 201 (2009) [arXiv:0704.0979 [astro-ph]] [Search INSPIRE].
[107] A. A. Abdo et al., Phys. Rev. Lett. **104**, 101101 (2010) [arXiv:1002.3603 [astro-ph.HE]] [Search INSPIRE].
[108] M. Ackermann et al., Astrophys. J. **799**, 86 (2015) [arXiv:1410.3696 [astro-ph.HE]] [Search INSPIRE].
[109] V. Berezinsky, A. Gazizov, M. Kachelriess, and S. Ostapchenko, Phys. Lett. B **695**, 13 (2011) [arXiv:1003.1496 [astro-ph.HE]] [Search INSPIRE].
[110] M. Ahlers, L. A. Anchordoqui, M. C. Gonzalez-Garcia, F. Halzen, and S. Sarkar, Astropart. Phys. **34**, 106 (2010) [arXiv:1005.2620 [astro-ph.HE]] [Search INSPIRE].
[111] G. B. Gelmini, O. Kalashev, and D. V. Semikoz, J. Cosmol. Astropart. Phys. **1201**, 044 (2012) [arXiv:1107.1672 [astro-ph.CO]] [Search INSPIRE].
[112] G. Decerprit and D. Allard, Astron. Astrophys. **535**, A66 (2011) [arXiv:1107.3722 [astro-ph.HE]] [Search INSPIRE].

[113] J. Heinze, D. Boncioli, M. Bustamante, and W. Winter, Astrophys. J. **825**, 122 (2016) [arXiv:1512.05988 [astro-ph.HE]] [Search INSPIRE].
[114] A. D. Supanitsky, Phys. Rev. D **94**, 063002 (2016) [arXiv:1607.00290 [astro-ph.HE]] [Search INSPIRE].
[115] D. Hooper, A. Taylor, and S. Sarkar, Astropart. Phys. **23**, 11 (2005) [arXiv:astro-ph/0407618] [Search INSPIRE].
[116] M. Ave, N. Busca, A. V. Olinto, A. A. Watson, and T. Yamamoto, Astropart. Phys. **23**, 19 (2005) [arXiv:astro-ph/0409316] [Search INSPIRE].
[117] D. Hooper, S. Sarkar, and A. M. Taylor, Astropart. Phys. **27**, 199 (2007) [arXiv:astro-ph/0608085] [Search INSPIRE].
[118] D. Allard, M. Ave, N. Busca, M. A. Malkan, A. V. Olinto, E. Parizot, F. W. Stecker, and T. Yamamoto, J. Cosmol. Astropart. Phys. **0609**, 005 (2006) [arXiv:astro-ph/0605327].
[119] L. A. Anchordoqui, H. Goldberg, D. Hooper, S. Sarkar, and A. M. Taylor, Phys. Rev. D **76**, 123008 (2007) [arXiv:0709.0734 [astro-ph]] [Search INSPIRE].
[120] R. Aloisio, V. Berezinsky, and A. Gazizov, Astropart. Phys. **34**, 620 (2011) [arXiv:0907.5194 [astro-ph.HE]] [Search INSPIRE].
[121] K. Kotera, D. Allard, and A. V. Olinto, J. Cosmol. Astropart. Phys. **1010**, 013 (2010) [arXiv:1009.1382 [astro-ph.HE]] [Search INSPIRE].
[122] M. Ahlers and J. Salvado, Phys. Rev. D **84**, 085019 (2011) [arXiv:1105.5113 [astro-ph.HE]] [Search INSPIRE].
[123] A. Aab et al., Astrophys. J. **804**, 15 (2015) [arXiv:1411.6111 [astro-ph.HE]] [Search INSPIRE].
[124] R. U. Abbasi et al., Astrophys. J. **790**, L21 (2014) [arXiv:1404.5890 [astro-ph.HE]] [Search INSPIRE].
[125] M. G. Aartsen et al., J. Cosmol. Astropart. Phys. **1601**, 037 (2016) [arXiv:1511.09408 [astro-ph.HE]] [Search INSPIRE].
[126] M. G. Aartsen et al., arXiv:1510.05228 [astro-ph.IM] [Search INSPIRE].